



Direct carbon fuel cell operation on brown coal



Adam C. Rady^a, Sarbjit Giddey^b, Aniruddha Kulkarni^b, Sukhvinder P.S. Badwal^{b,*}, Sankar Bhattacharya^a, Bradley P. Ladewig^a

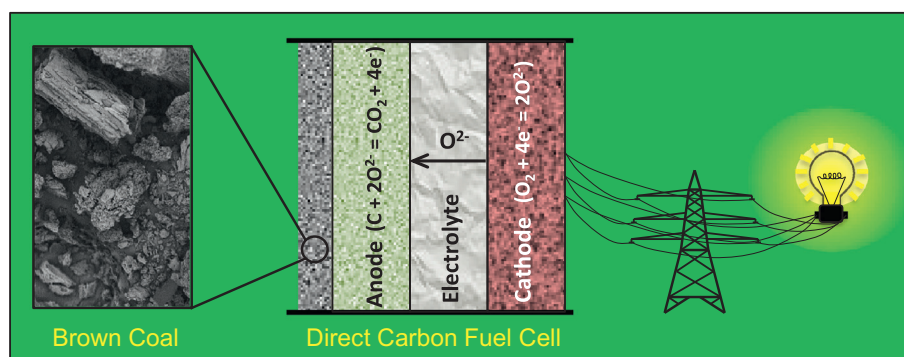
^a Department of Chemical Engineering, Monash University, Clayton, Australia

^b CSIRO Energy Technology, Private Bag 33, Clayton South 3169, Victoria, Australia

HIGHLIGHTS

- Performance of brown coal has been investigated in a direct carbon fuel cell.
- Fine particle size of the fuel is essential for better performance.
- The raw brown coal char gave superior performance due to a greater availability of CO at the anode.
- Inherent inorganic species in the raw coal catalysed the Boudouard gasification.
- Boudouard gasification kinetics of carbon fuels was compared using TGA.

GRAPHICAL ABSTRACT



ARTICLE INFO

Article history:

Received 23 September 2013

Received in revised form 4 December 2013

Accepted 11 January 2014

Available online 13 February 2014

Keywords:

DCFC
Fuel cell
Demineralsed coal
Brown coal
Lignite
Char

ABSTRACT

The performance of a Victorian brown coal with minimal pre-treatment was assessed in a solid oxide electrolyte based direct carbon fuel cell (DCFC) at 700 and 800 °C. In order to evaluate the effect of inherent inorganic species in the coal on the electrochemical performance of DCFCs (voltage – power density – current density), characteristics of button cells fuelled with raw and acid washed (demineralsed) coal were compared along with commercially available XC72 carbon black. Peak power densities of 65 and 67 mW cm⁻² were observed for demineralsed coal char and carbon black respectively at 800 °C, whereas the raw coal char achieved a superior power density of 89 mW cm⁻². The availability of reactive species at the anode, namely CO, is believed to be the primary differentiator of cell performance, and is related to variations in the physical and chemical makeup of carbon fuels. The reactivity of these fuels in the presence of CO₂ to generate CO (and power) via Boudouard gasification was assessed in the 700–800 °C temperature range via thermogravimetric analysis.

© 2014 Elsevier Ltd. All rights reserved.

1. Introduction

Fuel cells are able to generate electrical energy from fuels at high efficiency. Direct Carbon Fuel Cells (DCFCs) are the only such fuel cells capable of operating on a solid fuel, such as coal or biomass char, and can produce a product gas stream of concentrated CO₂ ideal for storage with minimal processing.

DCFCs offer the highest efficiency of any fuel cell type at near 100% theoretical efficiency at 600 °C for reaction (1) [1,2].



The direct carbon fuel cell efficiency (product of theoretical, voltage and fuel utilisation efficiencies) is around 80%, and overall system efficiencies (inclusive of system auxiliary losses) of above 60–70% have been projected [3]. Not limited by the Carnot cycle, the superior efficiency of DCFCs over conventional stationary coal-fired power generation could realise reductions in CO₂

* Corresponding author. Tel.: +61 395452719; fax: +61 395452720.

E-mail address: Sukhvinder.Badwal@csiro.au (S.P.S. Badwal).

emissions in the order of 50%, even without capture and storage. There is also scope for integration of DCFCs within other coal-based power generation technologies [4,5].

Reaction (1) is a familiar reaction in the oxidation or combustion of carbon and is also the overall reaction for a DCFC. However, the oxidation of carbon in a DCFC is electrochemical in nature and involves various intermediate reactions. These reactions may be electrochemical and/or thermochemical and depend on the DCFC type as well as reaction environment which the fuel is exposed to.

There are three main families of DCFC, which are commonly categorised depending on their electrolyte. These are the molten hydroxide, molten carbonate, and solid oxide DCFC. There are also sub-classes of the solid oxide electrolyte DCFCs depending on the physical arrangement of the fuel feed system and the anode. A detailed description of DCFC types can be found in a review by Giddey and co-workers [3].

For the solid oxide DCFC, oxygen is reduced at the cathode as per reaction (2).



Oxygen ions migrate across the electrolyte and oxidise carbon at the anode, releasing electrons back into the circuit (reaction (3)).



This is the overall anode reaction (not the complete mechanism of carbon oxidation), with intermediate reaction steps that may occur are given below:



The solid oxide DCFC is a high temperature fuel cell and operates between the temperatures of 600 and 900 °C, whereas the molten hydroxide and molten carbonate DCFCs are limited to operation below 800 °C partly due to the corrosive nature of their electrolytes amongst other factors such as the stability of the electrolyte and increasing vapour pressure at higher temperatures [6]. The high temperatures are necessary to ensure sufficiently high ionic conductivity of the ceramic electrolyte, but introduce other considerations, such as different reaction mechanisms and associated efficiency penalties. For example, at temperatures above 700 °C the reverse Boudouard reaction, hereinafter referred to as Boudouard gasification, becomes favourable when carbon dioxide is present (reaction (6)) [7,8].



Under these conditions, the fuel may be gasified and the fuel cell will operate off both the electrochemical oxidation of solid carbon (reactions (3) and (4)) and carbon monoxide available from reactions (4) and (6) as per reaction (5).

The mode of operation of the fuel cell is an important consideration for not only the performance, but also the efficiency of the system. Where reaction (6) is allowed to compete with reaction (4) for the consumption of carbon, some fuel may be lost as CO in the product gas, reducing the fuel utilisation and the overall efficiency of the system. For this reason Boudouard gasification is sometimes referred to as ‘Boudouard corrosion’ of the fuel, in the context of DCFC operation. Understanding what factors promote reaction (6), and its effect on the system, and how the fuel properties contribute, are necessary studies in advancing this technology.

Due to the difficult nature of tracking intermediate reaction products in the gaseous reaction environment, limited work has been done to elucidate the reaction mechanisms for the carbon oxidation in the solid oxide electrolyte based DCFC. A more detailed description of carbon conversion mechanisms in the solid

oxide DCFC for carbon deposited by CH₄ is given by Li and co-workers [9]. Their work outlined possible intermediate reaction steps such as the adsorption of oxygen onto the carbon surface, and the importance of carbon reactive sites. However, the interfacial conditions are expected to be quite different in a solid fuel fed DCFC compared to the methane fed solid oxide fuel cell.

Recent advances in DCFC technology as well as a greater understanding of the need for high efficiency and clean sources of power generation, has renewed interest in this area. However, the overwhelming fuel of choice for DCFC research to date is commercially produced carbon black [6,10–16] as it is considered a clean source of carbon with consistent properties. While carbon black has a lot to offer to this field of research, there is a need to explore the possibility of using real world fuels that would be traditionally used as fuels for DCFC to produce power at a commercial scale, such as coals, and expand knowledge on fuel-based performance of these fuel cells [17].

Coal is widely used for electricity generation worldwide, at over 40% of the global share, and its global consumption is expected to increase well into the next century [18]. In Victoria, Australia, brown coal is also the dominant fuel source for electricity generation contributing almost 80% to the total power generation installed capacity [19]. With around 33 billion tonnes [20] of ‘potentially economic’ reserves representing over 500 years of recoverable lignite at the current consumption rate, it is well positioned to retain this mantle for some time. However, it is widely accepted that the current methods of power generation have substantial negative environmental consequences. For example, the CO₂ emissions per MWh (more than 1.2 tCO₂/MWh [21]) of electricity produced in the Latrobe Valley, Victoria, are among the highest in the world. While the high moisture content of Victorian brown coal at 45–70% [22] is undesirable for thermal power generation, other properties such as its very low ash (<7 wt% db) and sulfur (<1 wt% db) contents make this coal an attractive fuel for use in fuel cells.

Amongst many challenges facing the development of DCFC technology, the delivery of a solid fuel to the effective reaction zones or triple phase boundaries for continuous operation of the fuel cell is the key issue for solid electrolyte based DCFC systems. One approach to overcome this problem is to mix solid fuel with a molten media such as molten carbonates and use traditional SOFC anodes such as Ni-YSZ (yttria-stabilised zirconia) to improve charge and ionic transfer between the anode and the solid fuel particles [15]. Anodes with low melting point metals such as Sn, Sb or Bi have also been trailed instead of molten carbonates in DCFCs with varying degree of success [23]. In short life-time experiments, these DCFCs demonstrate impressive performances, however, these systems present challenging technical issues such as rapid degradation of fuel cell components due to the corrosive nature of the molten media. In comparison, direct contact or fluidized bed type DCFCs potentially have fewer corrosion related issues during long-term operation. In these systems, particulate carbon is directly circulated on the anode surface or pressed onto the anode with external loading. Traditional SOFC anodes such as porous Ni/YSZ and Ni/SDC (samarium-doped ceria) cermets have been trialled in such DCFCs [24,25] with limited success, however, such anodes are unsuitable for continuous operation of a DCFC as discussed in a previous publication [8]. Recently promising power densities have been reported in DCFCs with single phase mixed ionic electronic conductor (MIEC) anodes such as (LaSr)(CoFe)O_{3-δ} (LSCF) and doped ceria [8,26]. MIEC anodes can carry O²⁻ ions to the anode surface thereby extending effective reaction zone beyond anode/electrolyte interface to anode/fuel interface thus facilitating the solid carbon oxidation on the anode surface itself.

The present work examines the performance of two processed coals from the Morwell mine in the Latrobe Valley, Victoria, in a

solid oxide electrolyte based DCFC using MIEC anode which has been shown to be stable in DCFC operating environments. Very few studies have involved the use of low rank coals within DCFCs to date and there is no reported data on the utilisation of Victorian (Australia) brown coal in this type of fuel cell. For comparison XC72 carbon black fuel was also investigated.

2. Experimental

Three carbons were used in this study. These were Cabot XC72 carbon black, and chars produced from demineralised Morwell coal and the parent (air-dried raw) Morwell coal, herein referred to as 'CB', 'DM', and 'RM', respectively.

2.1. Fuel preparation

To produce demineralised coal samples, 100 g of 150–212 μm air-dried raw Morwell coal was mixed with 2 L of 4 mol/L HNO_3 at a stirring rate of 80 rpm for 24 h at room temperature. The sample was then rinsed with no less than 20 L distilled water via Buchner funnel filtration until a constant pH of >4.0 was achieved. A neutral filtrate was not attainable due to inherent carboxyl and phenol groups lending the coal acidic properties.

The demineralised Morwell coal was then heated in a quartz fluidised bed reactor under an atmosphere of 99.999% N_2 flowing at 500 mL min^{-1} , at a heating rate of 10 $^\circ\text{C min}^{-1}$ to 600 $^\circ\text{C}$, where it was held for 1 h before cooling to room temperature to generate DM. The same process was employed for the parent coal, air-dried raw Morwell coal, to produce RM. The temperature of 600 $^\circ\text{C}$ was chosen as a temperature for removal of the majority of organic volatiles, but it was not sufficiently above the volatilisation temperature range of many inorganic salts for fluidised bed pyrolysis [27,28]. Thus most of the inorganic salts would still remain in the char sample. CB was not exposed to any heat treatment prior to use in the fuel cell or fuel analysis. A summary of the fuel preparation and treatment is given in Fig. 1.

2.2. Fuel characterisation and analysis

Thermogravimetric analysis (TGA), with a Netzsch STA449 F3 Jupiter, was used to assess weight loss due to release of volatiles in the charred samples, as well as investigate the reactivity of samples in the presence of CO_2 at fuel cell operating temperatures. For this investigation with TGA, a temperature profile closely representing fuel cell operation was selected. The temperature was increased from room temperature to 200 $^\circ\text{C}$ at 10 $^\circ\text{C min}^{-1}$, with all subsequent heating at 5 $^\circ\text{C min}^{-1}$ to 600, 700 or 800 $^\circ\text{C}$. A blank standard run with an empty crucible was subtracted from thermogravimetric profiles to account for buoyancy effects.

In a separate study, in order to determine volatile and moisture contents, carbon fuels were heated in the TGA furnace to 950 $^\circ\text{C}$ at heating rate of 10 $^\circ\text{C min}^{-1}$ in N_2 and held for 7 min at this temperature.

For all TGA work (both studies), samples (RM, DM and CB) were sieved to 90–106 μm size. Gases used were N_2 (99.999%) and ultra high purity CO_2 . A flow rate of 20 mL min^{-1} was used for the protective N_2 atmosphere with an additional 80 mL min^{-1} flow rate for the purge gas of either N_2 or CO_2 . Prior to each TGA run, the furnace chamber pressure was reduced to near-vacuum before being flushed with N_2 .

Inorganic content and make-up of coal samples were determined via inductively coupled plasma optical emission spectrometry (ICP-OES) analysis following microwave digestion of the char samples using a 6:1 HNO_3 and HF mix. These results were adjusted for metal oxide weights to give the ash content (see Section 3.1.1 below).

All coal samples were Au sputter coated prior to imaging with scanning electron microscope (Phenom S/N 0383 desktop SEM).

The conductivity measurements were made on compacted powders with a four-probe direct current technique at high temperatures in the 600–800 $^\circ\text{C}$ range in an inert atmosphere of nitrogen.

2.3. Cell fabrication

Ceria-Gadolinium Oxide (CGO, Fuel Cell Materials Inc., OH, USA) was used as the electrolyte material. The CGO powder (1.5 g) was uniaxially pressed in a die at 1 MPa for 60 s followed by isostatic pressing at 207 MPa (30 kpsi) for 30 s. The green electrolyte discs were then sintered at 1500 $^\circ\text{C}$ for 2 h in air with a heating rate of 300 $^\circ\text{C h}^{-1}$. The sintered discs had a diameter of 18 mm and were ~ 1 mm thick. Archimedes density measurements confirmed the discs to be $>98\%$ of the theoretical density. Lanthanum strontium cobalt ferrite (LSCF, Fuel Cell Materials Inc., OH, USA) with the composition $\text{La}_{0.6}\text{Sr}_{0.4}\text{Co}_{0.2}\text{Fe}_{0.8}\text{O}_{3\pm\delta}$, was used as both the air and fuel electrode. Its stability in direct carbon fuel cell environments and operating conditions has been demonstrated previously [13]. The electrode ink was made by ball milling LSCF powder and terpinol-based ink vehicle (Fuel Cell Materials Inc., OH, USA) in a 1:1 weight fraction for 4 h. An 8 mm diameter air electrode (cathode) was screen printed on one side, in the middle of the electrolyte discs and the entire opposite face of the electrolyte disc was brush painted with the fuel electrode (anode) ink. Electrodes were sintered at 800 $^\circ\text{C}$ for 2 h in air with a heating rate of 180 $^\circ\text{C h}^{-1}$. A thin coating of platinum ink (Metalor Technologies, Birmingham, UK) was applied to the air electrode prior to assembly to assist with current collection.

2.4. Fuel cell testing

A nickel crucible of dimensions 18.7 mm ID \times 19.0 mm OD \times 2.7 mm in depth was used to contain carbon fuel powder to be tested. A Platinum mesh of thickness 0.5 mm and diameter of 17 mm was spot welded to the bottom inside of this crucible. A Pt wire was spot welded to the mesh for current collection. Carbon fuels were ground in ethanol in a mortar and pestle to make a paste. This paste was then uniformly applied to the Platinum mesh with the help of a brush, in a way that the carbon paste is in level with the Platinum mesh top. The button cell was then placed on top of the platinum mesh and held in place by a spring-loaded alumina tube in an in-house designed button cell fixture. A schematic of the cell arrangement in the test fixture is shown in Fig. 2 as both assembled (a) and exploded view (b). Typical carbon loading was 50 mg with a different cell used for each carbon fuel type. Ceramabond-552 (Aremco Inc., NY, USA) sealant was cured *in situ* during the heating of the cell to isolate the air and fuel chambers. The fuel chamber was continuously purged under 99.999% N_2 for raw and demineralised Morwell chars, and 99.999% Helium for carbon black, at 40 mL min^{-1} flow rate during heating and normal

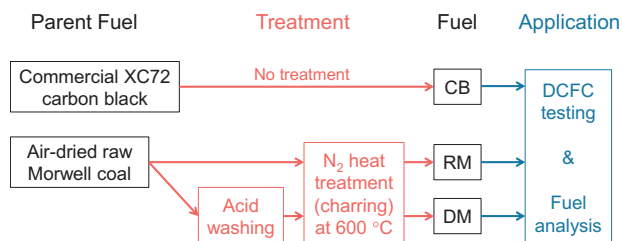


Fig. 1. Flow diagram of fuel preparation and utilisation.

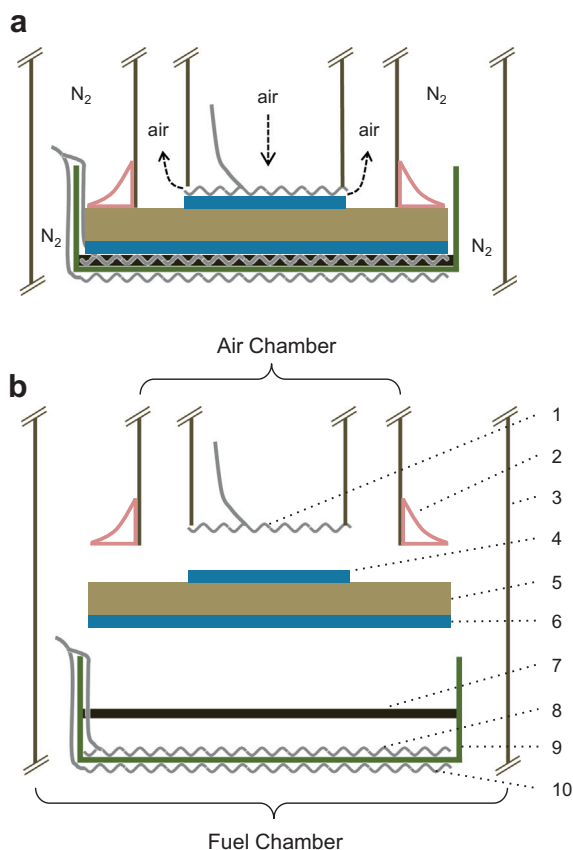


Fig. 2. Schematic of cell arrangement as (a) assembled diagram, (b) exploded view. (1) Cathode current collector (Pt mesh); (2) ceramabond seal; (3) alumina tube cell housing; (4) LSCF air electrode (cathode); (5) CGO electrolyte; (6) LSCF fuel electrode (anode); (7) carbon fuel; (8) anode current collector (Pt mesh); (9) Ni crucible and (10) Pt mesh.

operation. The cell temperature was raised to 100 °C in ambient air environment to assist with seal formation. The inert gas purge was then started, and temperature raised to 600 °C, at a heating rate of 300 °C h⁻¹. The cell was held at 600 °C for 1 h before ramping to operating temperatures of 700 and then to 800 °C for both coal chars. For carbon black, the cell was only operated at 800 °C. The cell holding time at a temperature during testing was typically 1 h with total cell operating time of about 2–3 h.

A Versastat 4 Potentiostat–Galvanostat (Princeton Applied Research, USA) was used to generate button cell polarisation curves. A two-electrode cell configuration was used and cells were loaded under potentiodynamic mode at a scan rate of 25 mV s⁻¹. Corrections to measured cell voltages were made for ohmic losses due to lead and Pt connecting wires. This was determined by shorting the air and fuel side connections at the cell operating temperatures. Electrochemical Impedance Spectroscopy (EIS) was conducted using an IM6 Impedance analyser (Zahner, Germany). The impedance spectra were recorded under open circuit conditions at an excitation voltage amplitude of 20 mV in the frequency range of 50 mHz–50 kHz after obtaining polarisation curves.

3. Results and discussion

3.1. Analysis of fuels

3.1.1. Proximate analysis and inorganic makeup of fuels

The moisture and volatile contents for all three fuels used in this study, as determined from heat treatment to 950 °C in the

TGA furnace, are given in Table 1. The ash content in Table 1 was determined from adjusted chemical analysis data (ICP–OES), with fixed carbon as the balance. The volatile contents of RM, DM and CB were 38.4 wt%, 29.3 wt% and 2.8 wt% respectively. It is quite clear from Table 1 that previous charring at 600 °C had not removed all volatile matter. As the samples were all heated to 950 °C for this analysis, volatilisation of some inorganic species, in particular those of sodium [27,28] may have contributed to weight loss although this contribution is believed to be minor compared with the weight loss due to organic volatile matter.

A similar moisture content of 2.4 and 2.6 wt% for RM and DM respectively was observed. It appears that the hygroscopic coal chars reabsorbed some moisture from the atmosphere post-charring at 600 °C. Acid leaching of the coal appears to have been successful in reducing the inorganic content of the fuel substantially, resulting in an ash content of 0.8 wt% for DM, considerably lower than the 2.6 wt% for RM, despite DM having the higher fixed carbon content. The ash content of CB was deemed negligible. Not surprisingly, the commercially produced CB had the highest fixed carbon content at 96.6 wt% due to low moisture, volatile matter and inorganic content. RM had the lowest fixed carbon content of 56.6 wt%, due mostly to a high volatile content.

The chemical analysis data of RM and DM (ICP–OES) are given in Table 2. Detailed analysis of both RM and DM chars indicated that the concentration of Ca, Mg and Fe was significantly high in RM but decreased considerably on acid leaching, by roughly an order of magnitude. Al content in DM was also substantially lower than in RM, suggesting its presence in RM is predominantly in the form of clays readily removed by acid leaching or rinsing. Though the specific mineral phases in the char samples were not determined, Si is well known to exist in forms resistant to mild acid treatment within coals and the majority of the residual Si in DM is usually in the form of stable quartz.

Na and K also showed a tolerance to acid treatment, despite their dominant presence in Victorian brown coal being in the form of salts and carboxylates which are easily removed via acid washing. The observed minor increase in K content in the DM sample may be a consequence of the sensitivity of the instrument. The residual Na in DM is in the form of sodium silicates, sulphate and nitrate. The nitrate results from the HNO₃ used during leaching and is difficult to remove completely despite intensive water washing following acid leaching. This also explains the relatively ineffective removal of S via acid leaching.

3.1.2. Assessment of volatile constituents of fuel

The TGA analysis, independent of that used in the proximate analysis described in Section 3.1.1, and more representative of the DCFC operating temperature profile is presented in Fig. 3. The weight loss was observed below the temperature of charring (600 °C) for both RM and DM samples. This weight loss is attributed primarily to incomplete charring of the coal. However, to a lesser extent, one can expect the release of additional volatiles upon reheating char as an unavoidable consequence of the nature of the coal. It is also important to note that these chars were produced by pyrolysis under N₂ atmosphere at 600 °C, and some weight loss for both coal samples above 600 °C can be attributed to the release of tars and other volatiles not removed below this

Table 1
Proximate analysis of carbon fuels (wt%).

| | Moisture | Volatile | Fixed carbon | Ash |
|----|----------|----------|--------------|-----|
| RM | 2.4 | 38.4 | 56.6 | 2.6 |
| DM | 2.6 | 29.3 | 67.3 | 0.8 |
| CB | 0.6 | 2.8 | 96.6 | – |

Table 2

Inorganic content of char samples as determined by ICP-OES (ppm as metals on dry basis).

| | Si | Al | Fe | Ti | K | Mg | Na | Ca | S | Other |
|----|-----|------|------|------|-----|------|------|------|------|-------|
| RM | 324 | 135 | 2100 | 22.0 | 570 | 2900 | 1600 | 6100 | 2400 | 261 |
| DM | 200 | 6.10 | 273 | 19.0 | 585 | 173 | 1000 | 538 | 1700 | 201 |

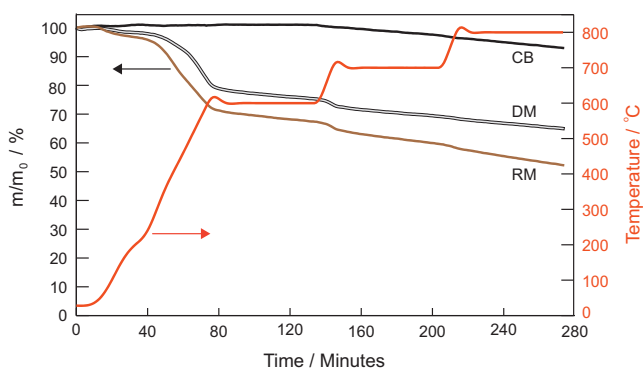


Fig. 3. Temperature profile and thermogravimetric mass loss curves for carbon fuel samples during thermal treatment under N_2 . m: sample mass at a given time; m_0 : initial sample mass.

temperature. This is observed in the temporary increase in rate of mass loss during heating from 600 to 700 °C for both DM and RM.

A linear weight loss during isothermal heat treatment at 700 and 800 °C in Fig. 3 for all fuels was also observed. Four potential contributors to weight loss under these conditions cannot be ruled out. These include loss of volatile content and volatilisation of fixed carbon; CO and CO_2 desorption from decomposition of oxygen functional groups; oxidation of carbon due to trace level of oxygen in the inert gas; and from ingress of air into system via an unidentified leak. Of these possible scenarios, it is likely that the continued release of volatiles at these elevated temperatures is a major contributor to the observed linear weight loss profile. In addition, the decomposition of surface functional groups, predominantly into CO, was observed for carbon black at temperatures above 700 °C in a temperature programmed desorption experiment by Li and co-workers [10]. This is consistent with the onset temperature for weight loss of CB in Fig. 3 and presents as a possible source of CO for utilisation in a fuel cell reaction. Contributions to weight loss via oxidation from inherent impurities in inert N_2 (rated at <2 ppm O_2 and <3 ppm H_2O) and air ingress are considered minor.

3.1.3. Boudouard gasification reactivity of fuels via TGA

The relative reactivity of carbon fuels to Boudouard gasification were inferred by comparing mass loss versus time upon exposure to CO_2 . This was achieved using thermogravimetric analysis (TGA) and a controlled atmosphere/temperature environment. The purge stream of 80 mL min^{-1} was switched from N_2 to CO_2 after 1 h at 700 °C or 800 °C as shown in Figs. 4 and 5 respectively. These figures compare rates of weight loss for RM and DM chars in the presence of N_2 and then CO_2 at 700 °C and 800 °C respectively. There was a significant loss of weight for both samples during heating in N_2 . This is attributed to loss of weight due to organic volatile not removed completely during charring as mentioned above.

For isothermal hold at 700 °C in N_2 , although there was some loss of weight with time, the rate of weight loss was relatively small (Fig. 4). However, on introduction of CO_2 into the furnace at ~145 min mark, the rate of weight loss for RM char became very notable (at 11.4 wt% over just first 15 min), leading to conversion of the reactive carbon with time as obvious in Fig. 4. The residual

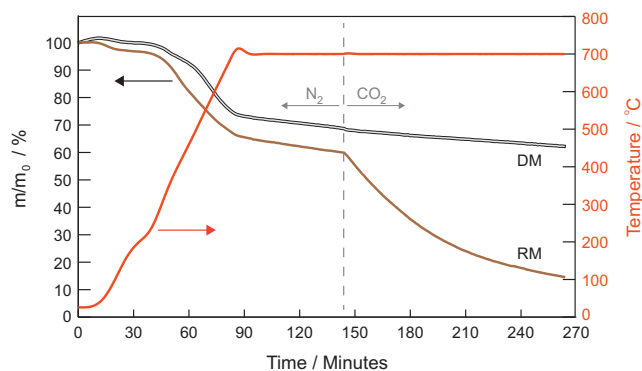


Fig. 4. Temperature profile and thermogravimetric mass loss curves for DM and RM during CO_2 gasification at 700 °C. m: sample mass at a given time; m_0 : initial sample mass.

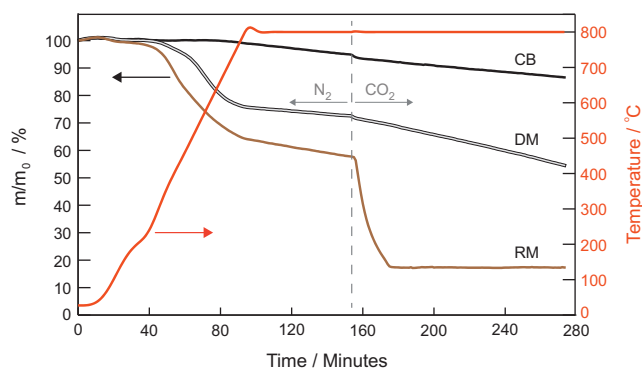


Fig. 5. Temperature profile and thermogravimetric mass loss curves for carbon fuels during CO_2 gasification at 800 °C. m: sample mass at a given time; m_0 : initial sample mass.

mass is attributed to ash content and smaller amount of unreacted carbon. This is not the case for DM, where the rate of mass loss under CO_2 flow is indistinguishable (1.31 wt% over first 15 min) from the previous isothermal stage under N_2 (1.15 wt% over the 15 min immediately prior to the introduction of CO_2).

As mentioned earlier, in the presence of CO_2 , the Boudouard gasification as per reaction (6) becomes favourable only beyond 700 °C. Above this temperature, CO becomes increasingly dominant gaseous species in the Boudouard gasification equilibrium reaction [7]. Although the kinetics of this reaction is poor at 700 °C or below for pure carbon, RM contains several inherent inorganics which are well known as catalysts for Boudouard gasification [29]. These inorganic species in RM char are in the form of Alkali and Alkaline Earth Metallic species (AAEM) and transition metals (see Table 2). It is highly likely that at 700 °C, catalysis of this reaction, as observed in the RM case, is taking place for the reaction to proceed at an appreciable rate. Therefore, mass loss in RM in the presence of CO_2 is attributed to the consumption of solid carbon via reaction (6). The TGA data also suggests minimal contribution to carbon consumption of the DM char via Boudouard gasification at this temperature [7]. This is attributed to the removal of catalytically active inorganic species and pore structure collapse during demineralisation of the coal [30].

In Fig. 5, the rates of weight loss for all carbons (CB, RM and DM) in the presence of N_2 and CO_2 at 800 °C are presented. The samples were heated in the presence of high purity N_2 and held for 1 h at 800 °C. The CO_2 was introduced after ~157 min from the start of the TGA run. The RM char was readily consumed within a few minutes via Boudouard gasification at this elevated temperature. DM showed a slightly enhanced rate of weight loss under CO_2

Table 3

The weight loss as wt% of samples over a 15 min period just before (in N₂), and after CO₂ purge at a given temperature in TGA analysis.

| | 700 °C (N ₂) | 700 °C (CO ₂) | 800 °C (N ₂) | 800 °C (CO ₂) |
|------------|--------------------------|---------------------------|--------------------------|---------------------------|
| CB | – | – | 1.02 | 1.04 |
| DM | 1.15 | 1.31 | 0.81 | 1.82 |
| RM | 1.45 | 11.42 | 1.61 | 31.48 |
| Figure | 4 | 4 | 5 | 5 |
| Time (min) | 126–141 | 144–159 | 135–150 | 157–172 |

(1.8 wt% in first 15 min) over that observed under N₂ (0.8 wt% over 15 min immediately prior to the introduction of CO₂) suggesting that this fuel reacted with CO₂ at this temperature although slowly. The CB sample, however, did not show any noticeable enhanced weight loss which could be attributed to carbon consumption via Boudouard gasification. It may be concluded that the reactivity of fuels in the presence of CO₂ decreases in the order of RM ≫ DM > CB. As mentioned above, the presence of inorganic species, namely AAEM and transition metals, appear to play a central role in differentiating reactivity of these fuels via the catalysis of reaction (6) at fuel cell operating temperatures of interest in this study. Furthermore, from the data in Table 2, it is apparent that of these species, Fe, Ca, and Mg are of most relevance due to their effective removal via acid leaching and their superior catalytic properties over other inorganic species present in the Victorian brown coal [30].

Table 3 summarises the rates of weight loss observed from the TGA results, as a wt% of initial sample weight over 15 min periods, both immediately before (in N₂) and after (in CO₂) introduction of CO₂ into the sample chamber at both 700 and 800 °C.

3.2. Conductivity data for fuels

The conductivity measurements on compacted powders, with a four-probe direct current technique at high temperatures, showed that RM was the most resistive followed by DM and CB. At 800 °C, the conductivity values for CB, DM and RM respectively were 1.0, 0.5 and 0.1 S cm⁻¹. Since the compacted powder density would be somewhat similar to that of carbon fuel used in direct carbon fuel cells, these results clearly show that mineral impurities in raw Morwell coal make substantial contribution to the resistivity of coal char and on acid leaching when most of these impurities are removed, the conductivity increases by a factor of about five.

3.3. Fuel cell results

Fig. 6 shows the voltage – power density – current density (V–P–I) characteristics for DCFC button cells operating on DM and RM chars at 700 °C. The two fuels achieved similar peak power densities at 37 and 38 mW/cm² for DM and RM respectively. Despite a marginally higher open circuit voltage (OCV) for RM, V–I and P–I curves almost overlap at current densities up to the peak power for DM. At higher current densities, there is a clear indication for the onset of a mass transfer limited process for the DM sample, whereas the RM showed no such behaviour in the V–I and P–I curves.

The reason for varying nature of the curves beyond the peak power is believed to be primarily related to findings in the TGA study in Section 3.1.3. As shown in the TGA investigation, the Boudouard gasification kinetics for RM is far superior to that of DM at temperatures around 700 °C (Fig. 4). With increasing current density, the direct contacting carbon cannot sustain the fuel cell reaction ($C + 2O^{2-} = CO_2 + 4e^-$) and mass transfer limitation occurs as is the case with DM. However, for RM, CO can be produced, via catalysis of reaction (6) by the inherently present impurities in

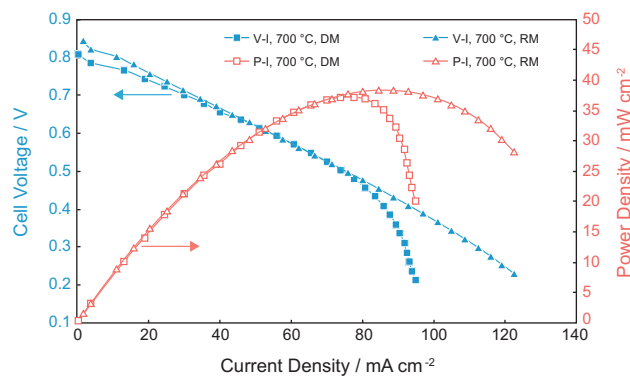


Fig. 6. Voltage – current density – power density curves for DM and RM using two similar LSCF/CGO/LSCF button cells at 700 °C.

RM char. This CO generated *in situ* then can react with migrating oxygen ions via reaction (5) thus sustaining the fuel cell operation.

Fig. 7 shows the V–P–I characteristics for DCFC button cells operating on DM, RM, and CB at 800 °C. At this temperature, again a mass transfer limited behaviour was observed for DM at higher current densities and close to the peak power density obtained for this cell, although, it was not as severe as that observed at 700 °C (Fig. 6). This may be attributed to enhanced reactivity of the fuel, including improved Boudouard gasification kinetics with increasing temperature. The best fuel cell performance was achieved for RM char followed by CB and the DM char. The cell with CB could be operated at much higher current densities and has a broader peak power range than DM. RM also exhibited a broad peak power range and the highest peak power density of any fuel tested here. The peak power densities at 800 °C for DM, CB and RM were 65, 67 and 89 mW cm⁻² respectively.

As was observed at 700 °C, Boudouard gasification reactivity at 800 °C (Fig. 5) is superior for RM over other fuels. This is a likely contributor to the higher current and power densities for RM, with a greater availability of CO at the anode. The extension of the V–I curve for DM beyond the peak power may also be due to DM showing improved gasification kinetics at 800 °C, with more evident weight loss under CO₂ atmosphere than at 700 °C, in the TGA studies.

It is not obvious why the cell with CB which had no mineral matter operated at much higher current densities and had a broader peak power range than DM. This may be attributed to a smaller particle size of CB and better flow characteristics as compared to DM. The Vulcan XC-72 (CB) is known to be a very high surface area material (250 m² g⁻¹) [31]. SEM images of three fuels in Fig. 8

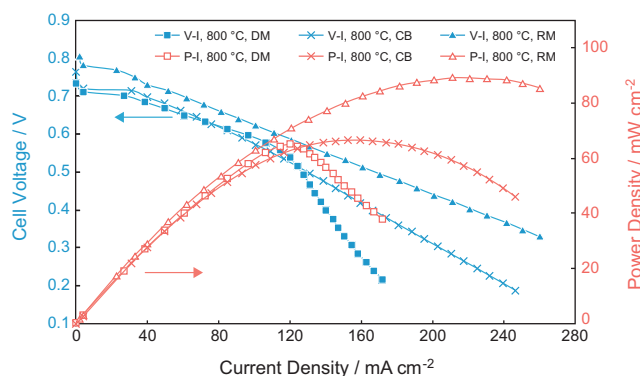


Fig. 7. Voltage – current density – power density curves for DM, RM, and carbon black (XC72) using three similar LSCF/CGO/LSCF button cells at 800 °C.

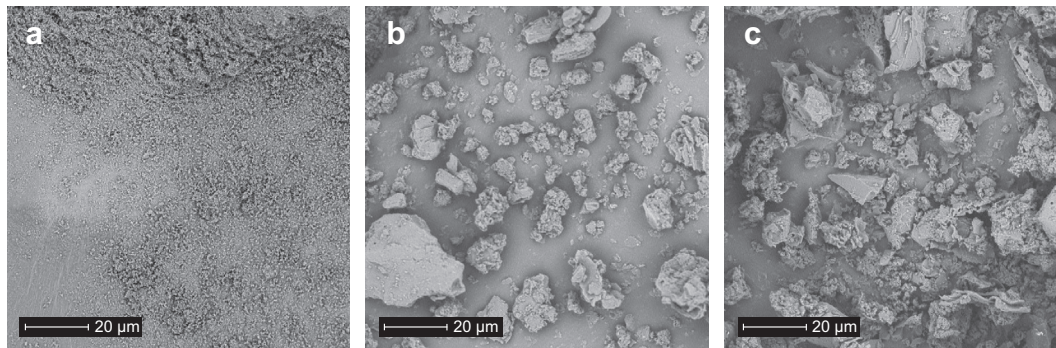


Fig. 8. Scanning electron micrographs of (a) carbon black, (b) demineralised Morwell char, (c) raw Morwell char.

clearly show that CB consists of much finer particles as compared to large agglomerates in DM and RM. A smaller particle size would enable better fuel to anode contact and increase the effective reaction zone. A greater number of fuel to anode points of contact per unit area may ensure the availability of fuel at relatively higher currents as compared to DM leading to a broader peak power range. In addition, the higher electrical conductivity of carbon black compared with RM and DM would extend the active anode area beyond the anode/fuel interface [13].

The button cells in the present test setup were under spring loading with an anode continuously pressed on the carbon fuel particles. In such a system it is reasonable to assume that finer CB particles would be in better contact with the anode leading to broader V–P–I characteristics. In the absence of catalysts, as is the case with CB and to some degree with DM char, the availability of the fuel through better contact with the anode is essential to get performance from a DCFC. Furthermore a smaller particle size may possibly improve the flow characteristics of CB fuel as compared to larger DM char particles which would provide continuous contacts of fresh fuel particles to the anode surface as the fuel is consumed with increasing current density.

It was observed that consistently cells with RM, both at 700 and 800 °C, showed higher OCV than cells with DM and carbon black (CB). Some variations from cell to cell are not uncommon due to the lack of perfect sealing. However, more significantly it appears that some mineral impurities in Raw coal facilitate Boudouard gasification of carbon with residual oxygen in the inert gas thus producing a small amount of CO and shifting the equilibrium to somewhat lower oxygen partial pressure giving rise to higher OCV. There was also an observed drop in the OCV with increasing temperature for both RM and DM samples. This is consistent with literature and is due to an increasing electronic conductivity of CGO in reducing environments with increasing temperature [8,32,33]. Nevertheless CGO has been shown to be a reasonably stable electrolyte material under a reducing environment of CO in a recent paper at temperatures similar to those used in this study [34].

Electrochemical impedance spectroscopy measurements performed on both coals at 700 and 800 °C showed the presence of more than one arc for the electrode behaviour. The mass transfer limitation experienced by DM at both temperatures is reflected in large low frequency arcs in the impedance spectra shown in Figs. 9 and 10. Such a behaviour has been observed before and modelled in a forthcoming publication [35]. It was related to Warburg-type diffusion limitation, the magnitude of which depends on the availability of fuel near the anode/electrolyte interface. The same type of model was applied here and the values of Warburg resistive component was 4.0 ohm-cm² (total cell resistance calculated from the model is 6.7 ohm-cm²) for DM char and 1.3 ohm-cm² (total cell resistance calculated from model is

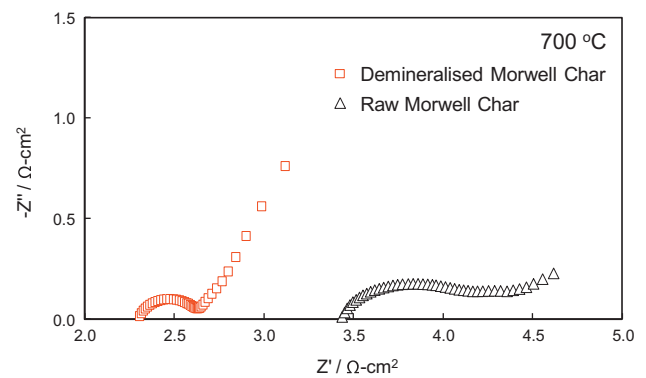


Fig. 9. Impedance spectra for DM and RM at 700 °C under open circuit voltage.

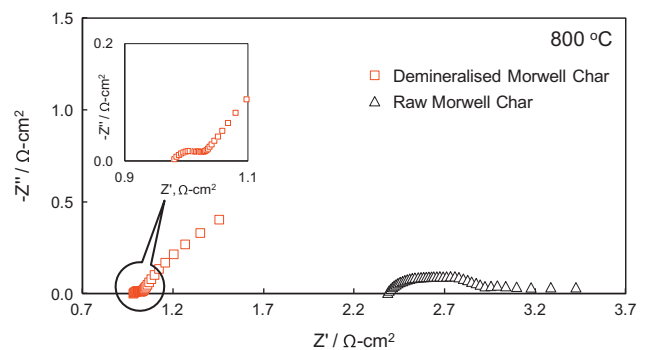


Fig. 10. Impedance spectra for DM and RM at 800 °C under open circuit voltage.

5.5 ohm-cm²) for RM char at 700 °C. These results are consistent with V–I data. With an increase in the DCFC operating temperature to 800 °C, there was a marked decrease in the size of both high and low frequency arcs and the value of Warburg resistive component decreased to 1.5 ohm-cm² (total cell resistance calculated from the model is 3.0 ohm-cm²) for the DM char. Due to the flat nature of the impedance curve for the diffusion arc, its magnitude could not be determined accurately for RM char at 800 °C. Therefore, the relatively low diffusion-type limitation and the superior power density (89 mW cm⁻² at 800 °C) of the direct carbon fuel cell with RM char as the fuel source, suggests that the cell behaviour is strongly dependent on fuel reactivity and availability of reactive species at the anode. Of the reactive species, CO may be more abundant at the anode when RM was used as the fuel in comparison to DM and CB. This is due to greater Boudouard gasification reactivity of RM fuel as outlined in Section 3.1.3. Carbon dioxide produced by the cell *in situ* via reaction (3) is more likely to react

with solid carbon via reaction (6) for the RM fuel. Thus contributions to enhanced cell performance via additional reaction pathways, such as the CO-shuttle mechanism [36,37], may be the primary differentiator between cell performance for a given fuel. Such phenomena are well reported in the literature as a result of an increase in availability of CO at the anode [11,14,38]. Two of these studies [11,14] also investigated the effect of adding Boudouard gasification catalysts, in the form of AAEM species, to the carbon black fuel and observed substantial increases in power densities of the cell. These findings are in line with the observations in this study, albeit for a different carbon-based fuel in partially charred coals.

It has been difficult to attribute the high frequency arc in the EIS spectra (Figs. 9 and 10) to any specific anodic or cathodic process for a two-probe electrode study, and can be possibly due to a combination of cathodic reduction of oxygen (reaction (2)) and direct electrochemical oxidation of carbon (reactions (3) and (4)). These are temperature dependent processes and polarisation resistances decreased with increasing temperature for both fuels RM and DM chars.

As with the EIS spectra at 700 °C (Fig. 9), the ohmic resistance component of the RM cell is significantly higher than that of the DM cell at 800 °C (Fig. 10). It should be noted that the ohmic resistance (left intercept of the high frequency arc) consists of the electrolyte resistance and contact resistances between carbon particles and anode, and between carbon particles and current collectors. In a DCFC, the carbon fuel itself can act as a current carrier in addition to the platinum mesh, and the number of contacts between fuel and anode and the char conductivity can have an effect on the overall ohmic resistance. As discussed above, the conductivity of RM (0.1 S cm^{-1}) was considerably lower than that of DM (0.5 S cm^{-1}). It is highly likely that lower levels of impurities such as Si, Fe and Mg in DM in comparison to RM and a smaller particle size of DM char would have contributed to observed lower ohmic resistance for DM by allowing better contact between fuel particles with fewer insulating phases.

4. Conclusions

Partially charred Morwell coal, from the Latrobe Valley, Victoria, both acid washed (DM) and raw (RM), were tested in a solid oxide electrolyte based DCFC. Their performances were evaluated against a commercially produced carbon black (CB) as a benchmark fuel. At 700 °C, the peak power densities of raw and demineralised Morwell chars were similar, at 37 and 38 mW cm^{-2} , respectively. The V–P–I curves showed remarkable similarity at low current densities, however, at 800 °C, the raw Morwell char achieved much higher power densities. At 800 °C, the demineralised Morwell char produced a comparable peak power density (65 mW cm^{-2}) to that of the carbon black (67 mW cm^{-2}), with raw Morwell char achieving 89 mW cm^{-2} . A comparison of power and current densities obtained with carbon black and demineralised Morwell char indicates that a fuel with finer particle size could improve contact between the fuel and the anode, therefore sustaining higher current densities culminating in a broader V–P–I characteristic. It has also been proposed that the superior performance achieved by the raw Morwell char was primarily due to a greater availability of CO at the anode. Catalysis of Boudouard gasification by inherent inorganic species in the raw coal char namely Fe, Ca, and Mg, was observed. These species, largely removed in the demineralised Morwell char, and not present in carbon black, could create such contrasting anodic atmospheres. Thermogravimetric analysis of the carbons at operating temperatures confirmed superior Boudouard gasification kinetics of raw Morwell char over the other fuels.

Acknowledgements

The authors would like to thank Dr Christopher Munnings for reviewing this paper. The work carried out in this paper was supported by Brown Coal Innovation Australia (BCIA), CSIRO Energy Flagship and Monash University.

References

- [1] Muthuel M, Jin X, Botte GG. Fuel cells – exploratory fuel cells|direct carbon fuel cells. In: Jürgen G, editor. Encyclopedia of electrochemical power sources. Amsterdam: Elsevier; 2009. p. 158–71.
- [2] Chien AC, Corre G, Antunes R, Irvine JTS. Scaling up of the hybrid direct carbon fuel cell technology. Int J Hydrogen Energy 2013;38:8497–502.
- [3] Giddey S, Badwal SPS, Kulkarni A, Munnings C. A comprehensive review of direct carbon fuel cell technology. Progr Energy Combust Sci 2012;38:360–99.
- [4] Gür TM. Critical review of carbon conversion in “Carbon Fuel Cells”. Chem Rev 2013 [Washington, DC, US].
- [5] Ordowich C, Chase J, Steele D, Malhotra R, Harada M, Makino K. Applying learning curves to modeling future coal and gas power generation technologies. Energy Fuels 2011;26:753–66.
- [6] Desclaux P, Nürnberger S, Rzepka M, Stimming U. Investigation of direct carbon conversion at the surface of a YSZ electrolyte in a SOFC. Int J Hydrogen Energy 2011;36:10278–81.
- [7] Gür TM, Huggins RA. Direct electrochemical conversion of carbon to electrical energy in a high temperature fuel cell. J Electrochem Soc 1992;139. L95–L7.
- [8] Kulkarni A, Giddey S, Badwal SPS. Electrochemical performance of ceria-gadolinia electrolyte based direct carbon fuel cells. Solid State Ionics 2011;194:46–52.
- [9] Li C, Shi Y, Cai N. Mechanism for carbon direct electrochemical reactions in a solid oxide electrolyte direct carbon fuel cell. J Power Sources 2011;196:754–63.
- [10] Li X, Zhu Z, Chen J, De Marco R, Dicks A, Bradley J, et al. Surface modification of carbon fuels for direct carbon fuel cells. J Power Sources 2009;186:1–9.
- [11] Li C, Shi Y, Cai N. Performance improvement of direct carbon fuel cell by introducing catalytic gasification process. J Power Sources 2010;195:4660–6.
- [12] Chen M, Wang C, Niu X, Zhao S, Tang J, Zhu B. Carbon anode in direct carbon fuel cell. Int J Hydrogen Energy 2010;35:2732–6.
- [13] Kulkarni A, Ciacchi FT, Giddey S, Munnings C, Badwal SPS, Kimpton JA, et al. Mixed ionic electronic conducting perovskite anode for direct carbon fuel cells. Int J Hydrogen Energy 2012;37:19092–102.
- [14] Liu R, Zhao C, Li J, Zeng F, Wang S, Wen T, et al. A novel direct carbon fuel cell by approach of tubular solid oxide fuel cells. J Power Sources 2010;195:480–2.
- [15] Nabae Y, Pointon KD, Irvine JTS. Electrochemical oxidation of solid carbon in hybrid DCFC with solid oxide and molten carbonate binary electrolyte. Energy Environ Sci 2008;1:148–55.
- [16] Cherepy NJ, Krueger R, Fiet KJ, Jankowski AF, Cooper JF. Direct conversion of carbon fuels in a molten carbonate fuel cell. J Electrochem Soc 2005;152. A80–A7.
- [17] Rady AC, Giddey S, Badwal SPS, Ladewig BP, Bhattacharya S. Review of fuels for direct carbon fuel cells. Energy Fuels 2012;26:1471–88.
- [18] Burnard K, Bhattacharya S. Power generation from coal – ongoing developments and outlook. International Energy Agency; 2011.
- [19] Economics BoRaE. Energy in Australia. Department of Resources, Energy and Tourism, Australian Government, 2012.
- [20] Industries DoEaP. Fact Sheet: Victoria, Australia, A principal brown coal province. State Government, Victoria, 2010.
- [21] Johnson TR. Future options for brown coal based electricity generation – the role of IDGCC. ANZSES – Destination Renewables. Melbourne, Australia, 2003. p. 371–80.
- [22] Allardice DJ, Chaffee AL, Jackson WR, Marshall M. Water in brown coal and its removal. In: Chun-Zhu L, editor. Advances in the science of Victorian brown coal. Amsterdam: Elsevier Science; 2004. p. 85–133 [Chapter 3].
- [23] Jayakumar A, Javadekar A, Gissinger J, Vohs JM, Huber GW, Gorte RJ. The stability of direct carbon fuel cells with molten Sb and Sb–Bi alloy anodes. AIChE J 2013;59:3342–8.
- [24] Li S, Lee AC, Mitchell RE, Gür TM. Direct carbon conversion in a helium fluidized bed fuel cell. Solid State Ionics 2008;179:1549–52.
- [25] Dudek M, Tomczyk P, Juda KL, Tomov R, Glowacki BA, Batty S, et al. Comparison of the performances of DCFC fuelled with the product of methane rf plasma reforming and carbon black. Int J Electrochem Sci 2012;7:6704–21.
- [26] Werhahn MG, Schneider O, Stimming U. Thin film gadolinia doped ceria (GDC) anode for direct conversion of carbon black particles in a single planar SOFC. ECS Trans 2013;50:73–87.
- [27] Quyn DM, Wu H, Bhattacharya SP, Li C-Z. Volatilisation and catalytic effects of alkali and alkaline earth metallic species during the pyrolysis and gasification of Victorian brown coal. Part II. Effects of chemical form and valence. Fuel 2002;81:151–8.
- [28] Quyn DM, Wu H, Li C-Z. Volatilisation and catalytic effects of alkali and alkaline earth metallic species during the pyrolysis and gasification of Victorian brown coal. Part I. Volatilisation of Na and Cl from a set of NaCl-loaded samples. Fuel 2002;81:143–9.

- [29] Tomita A, Ohtsuka Y. Gasification and combustion of brown coal. In: Chun-Zhu L, editor. *Advances in the science of victorian brown coal*. Amsterdam: Elsevier Science; 2004. p. 223–85 [Chapter 5].
- [30] Bhattacharya S, Kabir KB, Hein K. Dimethyl ether synthesis from Victorian brown coal through gasification – Current status, and research and development needs. *Progr Energy Combust Sci* 2013;39:577–605.
- [31] Antolini E. Carbon supports for low-temperature fuel cell catalysts. *Appl Catal B: Environ* 2009;88:1–24.
- [32] Wang S, Kato T, Nagata S, Kaneko T, Iwashita N, Honda T, et al. Electrodes and performance analysis of a ceria electrolyte SOFC. *Solid State Ionics* 2002;152–153:477–84.
- [33] Zha S, Xia C, Meng G. Effect of Gd (Sm) doping on properties of ceria electrolyte for solid oxide fuel cells. *J Power Sources* 2003;115:44–8.
- [34] Badwal SPS, Fini D, Giacchi FT, Munnings C, Kimpton JA, Drennan J. Structural and microstructural stability of ceria – gadolinia electrolyte exposed to reducing environments of high temperature fuel cells. *J Mater Chem A* 2013;1:10768–82.
- [35] Giddey S, Kulkarni A, Munnings C, Badwal SPS. Performance evaluation of a tubular direct carbon fuel cell operating in a packed bed of carbon. *Energy*, 2014.
- [36] Nakagawa N, Ishida M. Performance of an internal direct-oxidation carbon fuel cell and its evaluation by graphic exergy analysis. *Ind Eng Chem Res* 1988;27:1181–5.
- [37] Gür TM. Mechanistic modes for solid carbon conversion in high temperature fuel cells. *J Electrochem Soc* 2010;157:B751–9.
- [38] Tang Y, Liu J. Effect of anode and Boudouard reaction catalysts on the performance of direct carbon solid oxide fuel cells. *Int J Hydrogen Energy* 2010;35:11188–93.